Park, J., Lühr, H. (2012): Effects of sudden stratospheric warming (SSW) on the lunitidal modulation of the F-region dynamo. - Journal of Geophysical Research, 117, A9

DOI: 10.1029/2012JA018035

Effects of sudden stratospheric warming (SSW) on the lunitidal modulation of the F-region dynamo

Jaeheung Park[1] and Hermann Lühr[1]

Received 15 June 2012; revised 19 July 2012; accepted 14 August 2012; published 26 September 2012.

[1] The E-region dynamo in the equatorial ionosphere changes significantly during Sudden Stratospheric Warming (SSW) events. However, little is known about the modulation of the F-region dynamo by SSW events. During the SSW event of December 2001 the vertical current density in the daytime equatorial F-region, as observed by the CHAMP satellite, exhibited oscillations with a 13-day period. This period reflects the lunar tide in the CHAMP satellite data. Two independent drivers are known to contribute to the F-region vertical current: thermospheric zonal wind (F-region dynamo) and vertical electric field (E-region dynamo). The thermospheric zonal wind as observed by CHAMP was modulated in a similar way as the F-region vertical current. Vertical electric field in the equatorial F-region can be estimated from the magnetic and plasma/neutral observations of the CHAMP satellite. The obtained values also show quasi 13-day modulations. The thermospheric wind and vertical electric field drove the F-region vertical currents in opposite directions, and the polarity of the net current generally followed the former (F-region dynamo). From the observed phase delays of the 13-day oscillations we conclude that the F-region vertical current during the SSW event was not only modulated by the variation of the thermospheric wind but also by the variations of the E-region electric field and the F-region plasma density distribution.

Citation: Park, J., and H. Lühr (2012), Effects of sudden stratospheric warming (SSW) on the lunitidal modulation of the F-region dynamo, *J. Geophys. Res.*, *117*, A09320, doi:10.1029/2012JA018035.

1. Introduction

[2] It was early in the 1960's when the effect of the stratosphere on the ionosphere was first observed [e.g., *Brown and Williams*, 1971; *Brown*, 1975, and references therein]. Henceforth, however, little progress had been made until recently (see the review of *Stening* [1992, and references therein]). The historical solar minimum around 2008 created favorable conditions for observing stratospheric effects on the ionosphere. The ionosphere around the solar minimum was extremely quiet (i.e., largely free from spectacular variations caused by geomagnetic storms and substorms) so that the stratospheric effect can be easily identified and isolated. Moreover, tidal dissipation in the lower thermosphere is weak for solar minimum conditions [e.g., *Häusler et al.*, 2010; *Pancheva and Mukhtarov*, 2011], so that the waves coming from lower altitude region are detected more easily at higher altitudes than for solar maximum conditions. Since then researchers began to show increased interest in the stratosphere-ionosphere coupling.

[3] Using vertical plasma drift observed at the Jicamarca Radio Observatory (JRO) during the sudden stratospheric warming (SSW) event in 2008, *Chau et al.* [2009] reported that the drift exhibits large deviations from the long-term average. The deviation was semi-diurnal (upward in the morning and downward in the afternoon) and lasted for several days. *Chau et al.* [2009] attributed the stratosphere-ionosphere coupling to amplified planetary wave (PW) activity during the SSW, which modulates the daytime E-region dynamo and vertical plasma drift. The ionospheric modulation by SSW has also been observed in total electron content (TEC) data in America [*Goncharenko et al.*, 2010a, 2010b] and in Asia [*Liu et al.*, 2011], global TEC [*Pedatella and Forbes*, 2010; *Yue et al.*, 2010], F-region plasma density [*Lin et al.*, 2012], vertical plasma drift [*Anderson and Araujo-Pradere*, 2010; *Fejer et al.*, 2011; *Rodrigues et al.*, 2011], geomagnetic field observed by ground stations [*Yamazaki et al.*, 2012a, 2012b], equatorial electrojet (EEJ) observed by ground stations [*Sridharan et al.*, 2009; *Fejer et al.*, 2010], and EEJ measured by a satellite on a low-Earth orbit [*Fejer et al.*, 2010; *Park et al.*, 2012]. The phase of the semi-diurnal ionospheric modulation shifts to later local time (LT) sectors with a speed of 12 [hour]/15 [day] [*Goncharenko et al.*, 2010b; *Fejer et al.*, 2010, 2011]. For more details about the recent advances on this subject, readers are referred to the latest review paper by *Chau et al.* [2011].

[4] The papers listed above generally agree that enhanced PW during SSW can interact with the equatorial semi-diurnal tide, which modulates in turn plasma structures through the E-region dynamo. However, the source of the semi-diurnal

[1]GFZ, German Research Center for Geosciences, Potsdam, Germany.

Corresponding author: J. Park, GFZ, German Research Center for Geoscience, Section 2.3, Telegrafenberg, DE-14473 Potsdam, Germany. (park@gfz-potsdam.de)

0148-0227/12/2012JA018035

tide (to be amplified by PW) is still under debate. *Fejer et al.* [2010, 2011] and *Park et al.* [2012] suggested that the phase shift of the semi-diurnal modulations is consistent with the lunar phase. On the other hand, *Stening* [2011] argued against the lunar origin based on (1) longitudinal differences of the ionospheric response to the SSW and (2) existence of strong lunitidal signatures during non-SSW periods. *Liu et al.* [2010] and *Fuller-Rowell et al.* [2011] conducted extensive numerical simulations, but the lunar tides were not considered in their works. Especially, the results of *Fuller-Rowell et al.* [2011] show phase-shifting semi-diurnal variation, but the semi-diurnal lunar tide was not used as an input [*Chau et al.*, 2011]. *Yamazaki et al.* [2012a] showed significant correlation of the SSW and lunitidal variations of the geomagnetic field, but they also argued that the relationship is not a perfect one-to-one correspondence. Recently, *Fang et al.* [2012] reproduced ionospheric variations observed during the SSW in January 2009 without including the lunar tides as an input to the simulation.

[5] Though many new aspects have already been reported to elucidate the ionospheric response to SSW, they are generally related to the E-region dynamo. The SSW effect on the F-region dynamo has not been investigated in detail. According to the numerical simulations of *Liu et al.* [2010, Figure 7] F-region wind (and its dynamo action) has little effect on the vertical plasma drift in all LT sectors, but they noted that the result depends on the F-region conductivity. Further investigation of coupling between the F-region dynamo and SSW is still warranted.

[6] In this paper we investigate the SSW effects on the dayside F-region dynamo for the SSW event in December 2001, as observed by the Challenging Minisatellite Payload (CHAMP). The solar activity is high during that period ($180 < F_{10.7} < 270$), and the F-region vertical currents associated with the F-region dynamo [e.g., *Heelis et al.*, 2012] are expected to be strong [*Park et al.*, 2010]. In section 2 we present the observations. In section 3 the results are presented, which are discussed in section 4 in relation to previous studies. Conclusion will be drawn in section 5.

2. Observation

[7] From July 2000 to September 2010 CHAMP sampled ionospheric F-region features on its low-altitude (from 450 km after launch to <300 km before mission end) and polar (87° inclination) orbit. The orbit precessed slowly through different LT sectors at a rate of 1 hour per 11 days. A Fluxgate Magnetometer (FGM) and an absolute Overhauser Magnetometer measured the geomagnetic field. The readings of the two magnetometers are inter-calibrated to produce accurate Level 2 data with 1 s resolution. For our work the Earth's main, crustal, and magnetospheric fields represented by the Pomme6 model (http://www.geomag.us/models/pomme6.html) were subtracted from the observed B-fields to isolate ionospheric effects. From an on-board accelerometer we can estimate thermospheric neutral mass density and zonal neutral wind in the east-west direction. Note that the uncertainty of the neutral wind observations of CHAMP is about 20 m/s [*Liu et al.*, 2006] when averaged over 10 s. The Planar Langmuir Probe (PLP) provides a plasma density reading every 15 s.

[8] Figure 1 presents CHAMP observations during a mid-winter SSW event in December 2001. Along the horizontal axis of Figure 1 time is given in the format of month/day. The panels from top to bottom exhibit (a) LT of the CHAMP orbit, (b) zonal neutral wind velocity (positive eastward), (c) zonal deflection of the B-field (eastward deflections are pointing to the right), (d) deviations of the B-field strength from the Pomme6 model field (strength enhancements are pointing to the right), (e) the high-latitude stratospheric temperature difference, (f) K_p index of daily average, and (g) $F_{10.7}$ index. For the stratospheric temperature the ERA-INTERIM re-analyses data of the European Centre for Medium-Range Weather Forecasts (ECMWF) is used [*Dee et al.*, 2011]. The data in Figures 1b–1d are moving bin-averages over 1° MLAT by 3-day (advancing by 1 day) cells, irrespective of geographic longitude (GLON). For example, for a given MLAT bin, the value for 21 December 2001 is an average of all the corresponding data from 20 to 22 December 2001. From Figure 1e we can see that the SSW event began around 23 December 2001. In Figure 1d we see the typical signature of the equatorial magnetic field (signature of the EEJ current [*Lühr et al.*, 2004]): the southward field deflections around the equator. The EEJ signature weakens between 23 and 31 December, right after the SSW. The southward deflections recover after 31 December, but decrease again to reach a local minimum near 10 January. This temporal variation has a period of about 13 days, which was also found in the CHAMP data in *Park et al.* [2012, Figure 1]. In Figure 1c the zonal B-field exhibits clear bipolar structures (eastward/westward in the northern/southern hemisphere, respectively) after 31 December, which corresponds to the F-region vertical currents, related to the westward thermospheric neutral wind (the F-region dynamo) [*Lühr and Maus*, 2006; *Park et al.*, 2010]. Between 23 and 31 December 2001 the bipolar structure cannot be easily identified because it is masked by strong unipolar magnetic structures (with the maximum at the magnetic equator), which represent the interhemispheric field-aligned currents [*Park et al.*, 2011]. Just like the parallel component of the B-field at the equator (Figure 1d), the bipolar structure of the zonal B-field (Figure 1c) exhibits a clear 13-day modulation. In Figure 1b the zonal neutral wind around the magnetic equator shows also periodic temporal variations similar to those of the magnetic field deflections. In the LT sector sampled by CHAMP during the SSW period the wind direction is generally westward, consistent with the polarity of the F-region vertical currents, as expected around noon time [*Lühr and Maus*, 2006; *Park et al.*, 2010]. The plasma density, as measured by the CHAMP/PLP (not shown here), also shows for this time interval that the crest-to-trough ratio (CTR) of the Equatorial Ionization Anomaly (EIA) exhibits significant 13-day variations [*Ritter et al.*, 2012]. Note that the K_p (Figure 1f) and $F_{10.7}$ (Figure 1g) indices do not exhibit a clear 13-day periodicity which can explain the variations of the EEJ, F-region current, and neutral wind as observed by CHAMP. Similarly, variations of solar wind speed during the

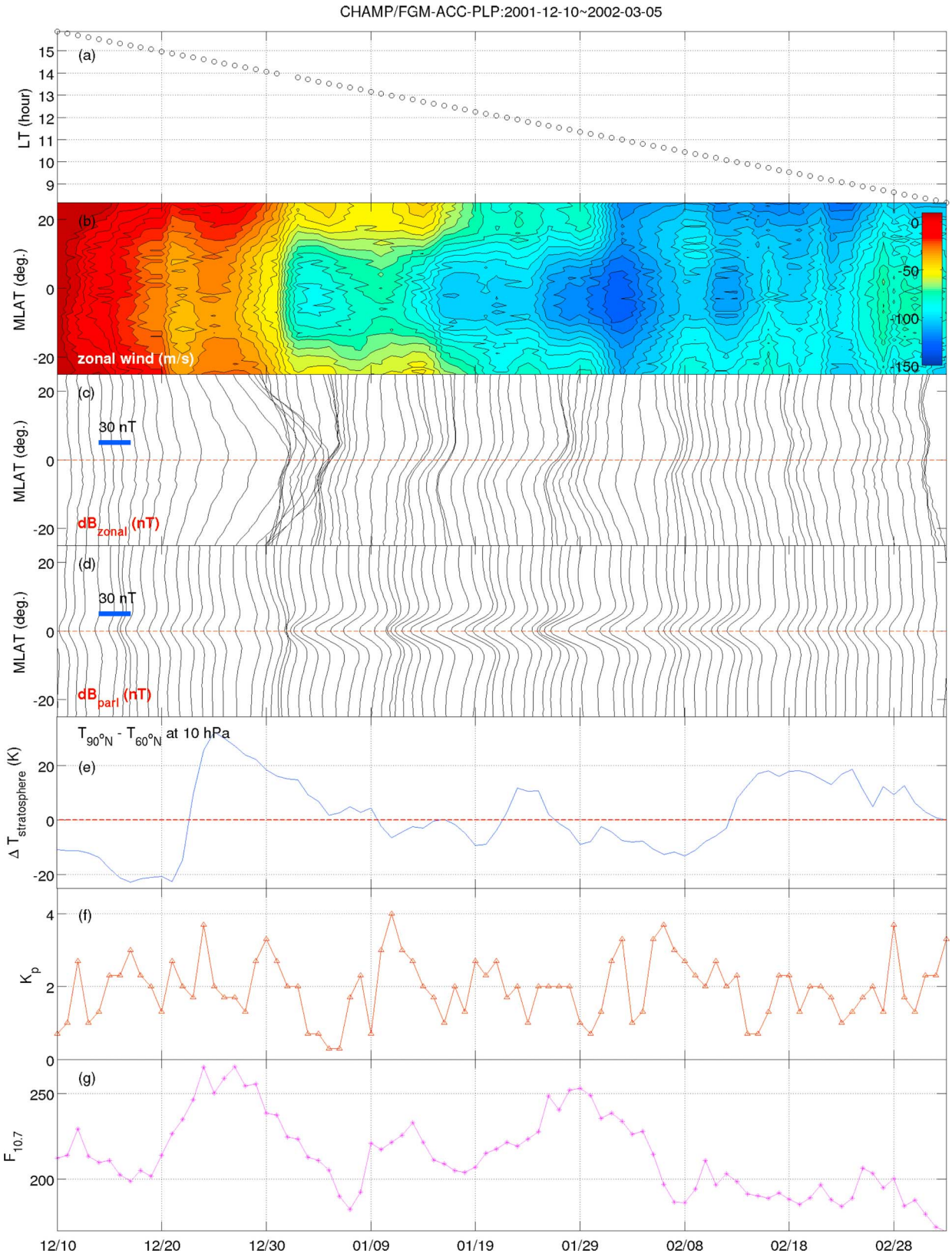

Figure 1. CHAMP observation during the SSW in December 2001: (a) local time variation of the CHAMP orbit, (b) zonal neutral wind (positive eastward), (c) zonal deflection of B-field (eastward is pointing to the right), (d) parallel component of B-field (strength enhancements are pointing to the right), (e) stratospheric temperature difference between the North Pole and 60°N, (f) K_p index of daily average, and (g) $F_{10.7}$ index.

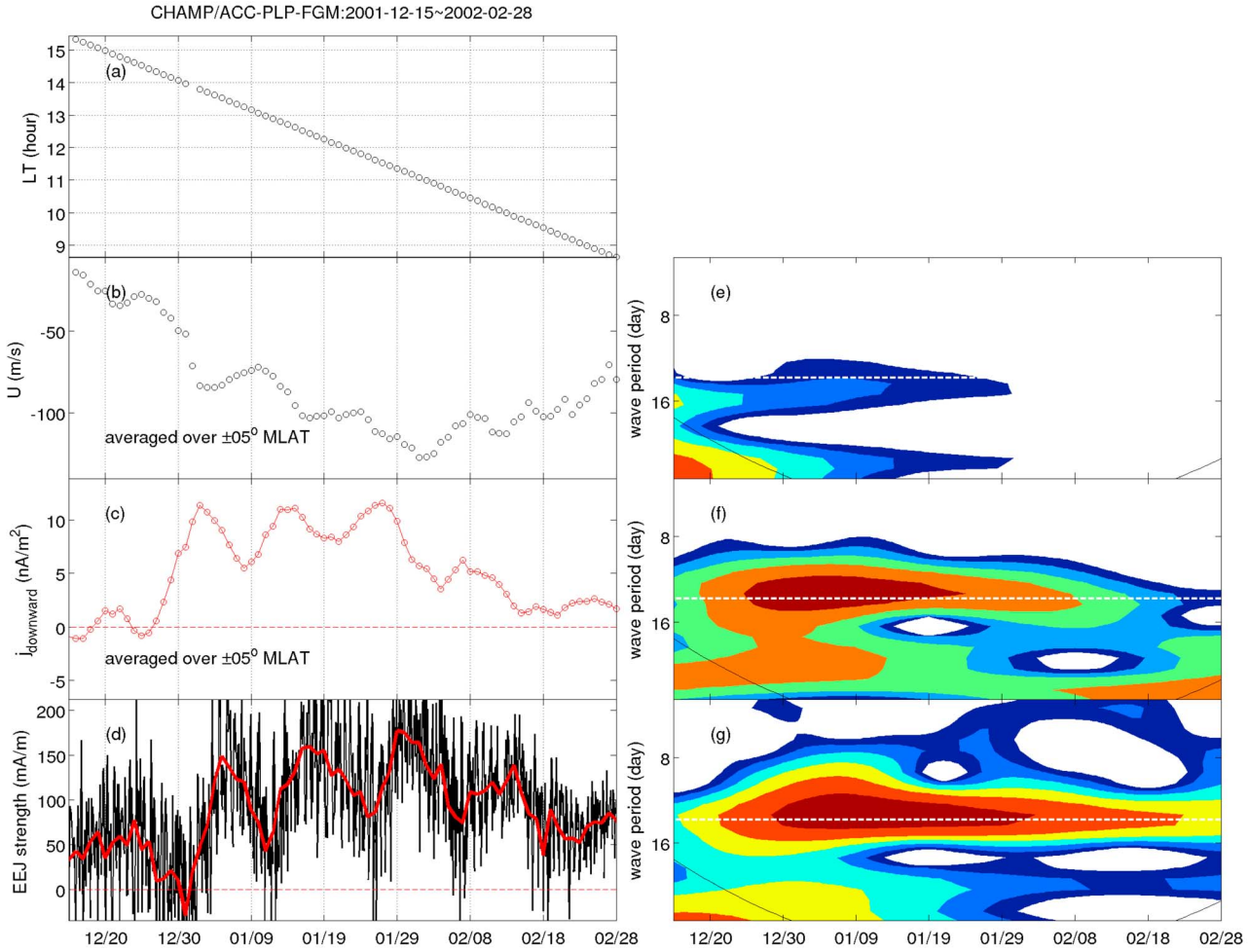

Figure 2. Processed CHAMP observations during the SSW event in December 2001: (a) local time of the CHAMP orbit, (b) zonal neutral wind averaged over ±5° MLAT, (c) F-region vertical current density averaged over ±5° MLAT, and (d) EEJ current strength. (e–g) Wavelet power spectra of Figures 2b–2d, respectively. The black lines denote the cone of influence, and the white dashed line corresponds to the 13.26-day period, which is the period of the semi-diurnal lunar tide as seen by CHAMP.

event, which is shown in *Park et al.* [2012, Figure 1], cannot explain the CHAMP observations.

3. Results

[9] Let us estimate the vertical current density, j_z, in the F-region using the CHAMP/FGM data. As we are interested in the near-equatorial region, we use a coordinate system defined as follows. The x-axis lies in the horizontal plane pointing toward geomagnetic north, y-axis also horizontal and toward geomagnetic east, and the z-axis points radially downward (toward the Earth's center). Ampere's law in this coordinate system is:

$$\nabla \times \mathbf{H} = \mathbf{j}$$

$$\left(\frac{\partial B_y}{\partial x} - \frac{\partial B_x}{\partial y}\right) = \mu_0 j_z.$$

If we neglect the y dependence by assuming a current sheet elongated in y direction, we obtain

$$\frac{\partial B_y}{\partial x} \approx \mu_0 j_z. \qquad (1)$$

Hence, from the latitudinal gradient of B_y we can estimate the (vertically) downward current density, j_z. For each day of interest we construct the longitudinally averaged latitude profile of B_y (see Figure 1c), and extract the latitudinally anti-symmetric component from the profile [*Park et al.*, 2010]. The latitudinal gradient of the anti-symmetric component is estimated near the magnetic equator to get a value of j_z for each day. The results averaged over ±5° MLAT are given in Figure 2c. Note that this approach is slightly different from that used by *Lühr and Maus* [2006] and *Park et al.* [2010] where they estimated the strength of the F-region dynamo sheet current density (in A/m).

[10] Equally, we have averaged the zonal wind (see Figure 1b) near the equator, which is shown in Figure 2b. The EEJ strength can be extracted from the B-field strength variation with respect to the Pomme6 model according to *Lühr et al.* [2004]. Results are shown in Figure 2d. The peak EEJ current strength from each dayside equatorial pass of CHAMP is shown as a black line in Figure 2d, with its daily average overplotted as a red line. Figure 2a again shows the LT progression of the CHAMP orbit. Figures 2e–2g

correspond to wavelet power spectra of the standard score of the signals shown in Figures 2b–2d, respectively. The black solid curves denote the cone of influence, and the white dashed lines correspond to the 13.26-day period, which is the period of the semi-diurnal lunar tide in the CHAMP orbit frame [*Park et al.*, 2012]. After the SSW onset on 23 December the EEJ strength (Figure 2d) starts to show strong modulations with a period of about 13 days, as is clearly seen in Figure 2g. The F-region vertical current density (Figure 2c) exhibits similar modulations at about 13 days, as seen in Figure 2f. The equatorial zonal wind is also modulated in a similar way after the SSW onset. Consistently, Figure 2e shows significant wave power around the 13-day period at least until 15 January 2002 (see also Figure 2b).

4. Discussion

4.1. Calculation of the F-Region Vertical Currents

[11] The daytime F-region vertical current density at the equator is generated by the interaction between the E-field, F-region conductivity, thermospheric zonal wind, and ambient B-field strength. Hence, we have an alternative way to estimate j_z. The local current density at a point in the F-region can be expressed as:

$$\sigma_P\left(\mathbf{E_{perp}} + \mathbf{u} \times \mathbf{B}\right) = \mathbf{j},$$

where σ_p is the local Pedersen conductivity in the F-region, $\mathbf{E_{perp}}$ is the F-region electric field perpendicular to the magnetic field, $\mathbf{u}$ is neutral wind, and $\mathbf{B}$ the ambient geomagnetic field. The first and second terms in parenthesis on the left-hand side correspond to the Pedersen currents driven by the F-region polarization E-field and by the F-region wind dynamo, respectively. As the F-region dynamo is known to generate a limited polarization electric field on the dayside, the first term in parenthesis of the left-hand side plausibly corresponds to the polarization electric field mapped up from the E-region dynamo. Near the equator the z direction (vertically downward) can be deemed as perpendicular to the ambient geomagnetic field. Then,

$$\sigma_P\left(E_z - u_y B_x\right) \approx j_z.$$

The local Hall conductivity is considered negligible because we are interested in the F-region. Note that j_z in the above equation reflects the current density that is estimated by equation (1) using the CHAMP/FGM data.

[12] If we neglect the electron contribution and assume that $\nu_{in}^2 \ll \Omega_i^2$ at this altitude, the Pedersen conductivity can be approximated as:

$$\sigma_P \approx \frac{n_e e^2 \nu_{in}}{m_i\left(\nu_{in}^2 + \Omega_i^2\right)} \approx \frac{n_e e^2 \nu_{in}}{m_i \Omega_i^2} = \frac{n_e m_i \nu_{in}}{B^2},$$

where n_e is the plasma density, e the electron charge, ν_{in} ion-neutral collision frequency, Ω_i ion gyrofrequency, and m_i the mean ion mass.

[13] For the ion-neutral collision frequency between O^+ and O, *Schunk and Nagy* [2009, Section 4.8, Table 4.5] provided an approximation:

$$\nu_{in} \approx 3.67 \times 10^{-17} n_n \sqrt{T_r}(1 - 0.064\ \log_{10} T_r)^2,$$

where n_n is the neutral density in m^{-3}, T_r the average of neutral (T_n) and ion (T_i) temperatures in Kelvin, and ν_{in} is given in s^{-1}.

[14] Hence, the vertically downward current density, j_z, as observed by CHAMP can be expressed as:

$$\begin{aligned} j_z &\approx \sigma_P\left(E_z - u_y B_x\right) \\ &\approx \frac{n_e m_i \nu_{in}}{B^2}\left(E_z - u_y B_x\right) \\ &\approx 3.67 \times 10^{-17} n_n \sqrt{T_r}(1 - 0.064\ \log_{10} T_r)^2 \frac{n_e m_i}{B^2} B_x \left(\frac{E_z}{B_x} - u_y\right). \end{aligned} \quad (2)$$

For this equation the plasma density n_e is measured by the CHAMP/PLP, and the magnetic field B_x and B by the CHAMP/FGM. As the other parameters (m_i, n_n, T_r, and E_z/B_x) are not directly provided by CHAMP, the following assumptions are made:

[15] 1. We assume that the ionosphere at CHAMP altitude is dominated by oxygen ions so that $m_i \approx 16 \times m_p$ where m_p is the proton mass.

[16] 2. We assume that the thermosphere at CHAMP altitude is also dominated by atomic oxygen. Then, neutral number density n_n can be estimated from the neutral mass density as derived from the CHAMP accelerometer.

[17] 3. We assume that T_i = 1000 K, a value consistent with the model of *Köhnlein* [1986] for daytime, and that T_n = 1000 K. Then, $T_r = \frac{1}{2}(T_i + T_n) = 1000$ K.

[18] 4. We assume that u_y can be approximated by cross-track wind as measured by CHAMP.

[19] With those assumptions we can estimate values for E_z/B_x from equation (2):

$$\begin{aligned} \frac{E_z}{B_x} &= u_y + \frac{j_z B^2}{3.67 \times 10^{-17} n_n \sqrt{T_r}(1 - 0.064\ \log_{10} T_r)^2 n_e m_i B_x} \\ &\approx u_y + \frac{j_z B^2 m_n}{3.67 \times 10^{-17} \rho \sqrt{T_r}(1 - 0.064\ \log_{10} T_r)^2 n_e m_i B_x}, \end{aligned} \quad (3)$$

where ρ is neutral mass density as observed by CHAMP, and m_n is mean mass of neutral particles. The results around the equator are shown in Figure 3. Figures 3a and 3b are the same as in Figure 2. For comparison, the EEJ strength for each orbit is shown as a black line in Figure 3f, with its daily average overplotted as a red line. Figure 3e corresponds to j_z as observed by the CHAMP/FGM while Figure 3c shows the related eastward plasma velocity, E_z/B_x at the equator as calculated from equation (3). The E_z/B_x curve in Figure 3c qualitatively follows that of eastward neutral wind (Figure 3b). E_z/B_x also seems to be affected by the quasi 13-day oscillations. Though this oscillation is not conspicuous in Figure 3c, its spectrum (figure not shown; the method used to get the spectrum is described in the next subsection) exhibits the peak amplitude around the 13-day period. On a larger temporal scale (>13 days), the behavior of E_z/B_x generally follows the LT variation of zonal plasma drift in the equatorial F-region above the JRO as shown in *Fejer et al.* [2005, Figure 5]. That is, the westward drift speed is largest slightly before local noon, and the direction remains westward within 09–15 LT. Only the magnitude of E_z/B_x in our Figure 3 is larger than that of *Fejer et al.* [2005] by about a factor of two.

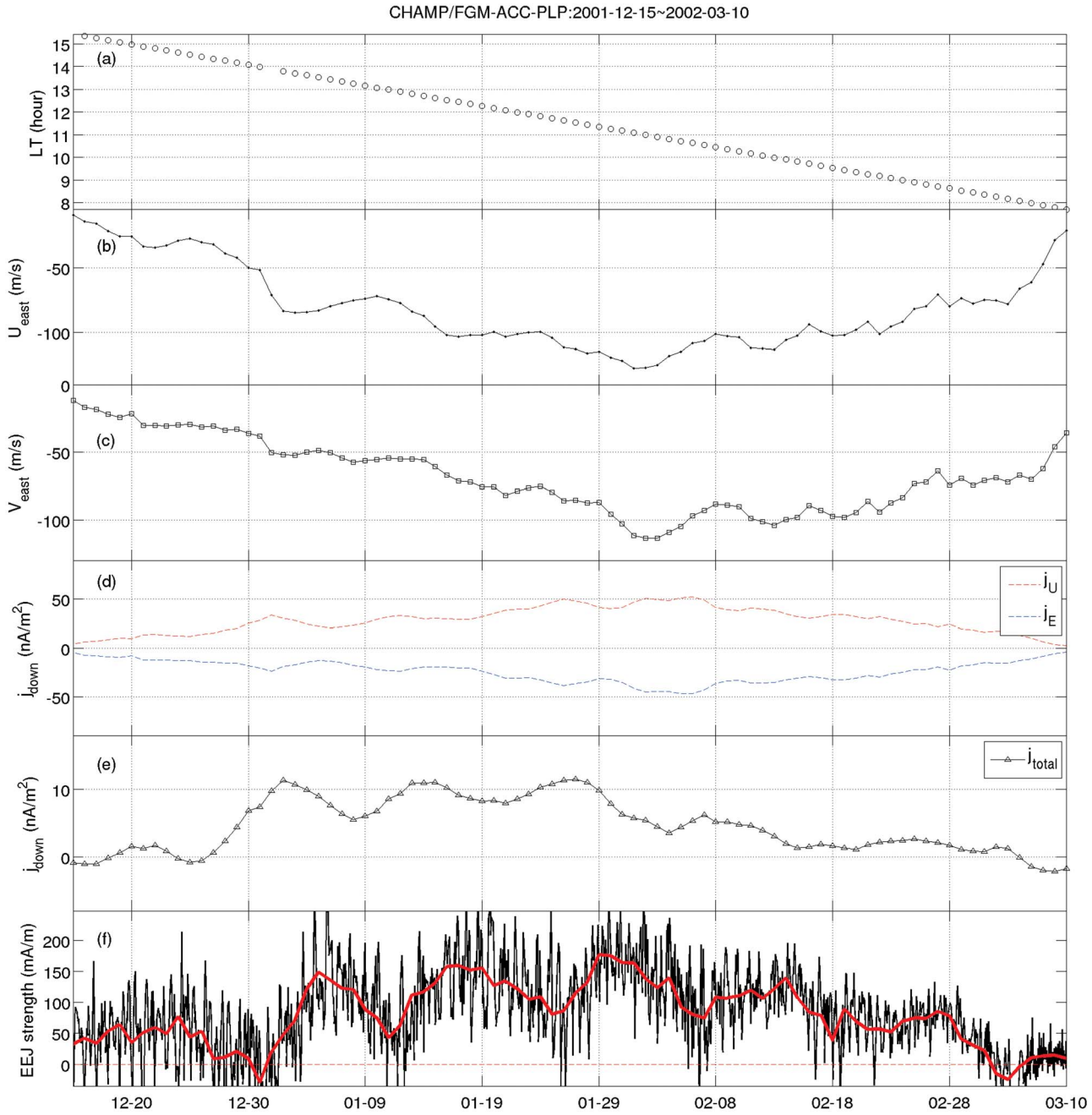

Figure 3. Compilation of observed and derived quantities. (a) Local time of CHAMP orbit, (b) thermospheric zonal wind, (c) eastward plasma drift (E_z/B_x) as calculated from the parameters observed by CHAMP, (d) downward current densities driven by thermospheric zonal wind (j_U) and by vertical E-field as a black line (j_E), and (e) net downward current. (f) For reference the EEJ strength for each orbit is shown as black line, with its daily average overplotted as a red line.

[20] The assumptions 1–4 shown above may partly be responsible for the magnitude discrepancy of E_z/B_x values between our results and those of *Fejer et al.* [2005]. In Figure 3c the minimum and maximum values of the estimated eastward drift speed are −113.5 m/s and −11.5 m/s, respectively. First, we check the sensitivity of the eastward drift speed on ion temperature (assumption 3). The ion temperature at the magnetic equator predicted by the International Reference Ionosphere model 2007 (IRI-2007) (http://omniweb.gsfc.nasa.gov/vitmo/) is generally higher than our assumption (1000 K), but below 1300 K during this SSW event. The neutral temperature at the magnetic equator predicted by the Mass Spectrometer Incoherent Scatter (MSIS) Model (http://omniweb.gsfc.nasa.gov/vitmo/) is in general below 1700 K during the same period. Even though we assume T_r = 1700 K, this temperature adjustment will enhance the plasma drift speed only by <3 m/s. Deviating from the assumptions 1

Table 1. Lunitidal Phase Delay of Ionospheric Parameters Related to the Downward Currents in the Equatorial Dayside F-Region

Signal	Tidal delay (days)	Tidal Delay (lunar hours)
Equatorial electrojet	4.7	3.8
Crest-to-trough ratio	3.4	2.7
Eastward drift	11.6(= −3.2)	9.4(= −2.6)
Westward wind	2.7	2.2
F-region downward current	0.6	0.5

and 2 we may have a certain admixture of heavier ions and neutrals. But, these two effects compensate each other (see equation (3)) and do not contribute significantly to the obtained drift velocity. It is finally the uncertainty in neutral wind measurement that directly affects the obtained plasma drift speed (see equation (3)). Error bars of ±20 m/s have been reported by *Liu et al.* [2006] for CHAMP neutral wind data. The remaining discrepancy may be attributed to the solar activity difference between our case ($169 < F_{10.7} < 266$, mean $F_{10.7} \approx 214$) and *Fejer et al.* [2005, Figure 5] ($F_{10.7} \approx 180$). Also, the discrepancy may partly be because the *Fejer et al.* [2005] results were obtained at one location (JRO) while we have considered longitudinal averages.

[21] Although CHAMP/DIDM could have directly measured the plasma drift velocity, its degradation during the launch prevents us from using in-situ observations of E_z/B_x. *Swarm*, an upcoming satellite mission of the European Space Agency (ESA) consists of three identical satellites with payloads similar to those on CHAMP. The *Swarm* satellites can measure the unknown quantities in equation (2), such as m_i, T_i, and E_z/B_x. Then, the consistency can be directly checked between the F-region vertical current density values estimated by the magnetic field observations (equation (1)) and by plasma/neutral observations (equation (2)). This test is left as a future work.

[22] Figure 3d shows the current contribution of the thermospheric zonal wind (Figure 3b) and that of the eastward plasma velocity, E_z/B_x (Figure 3c): the two add to the net downward current density, as deduced from the CHAMP/FGM (Figure 3e). The westward wind on the dayside (Figure 3b) drives downward currents (red line in Figure 3d) around the equator. On the other hand, the daytime westward plasma drift (Figure 3c) corresponding to the upward E-field drives an upward Pedersen current (blue in Figure 3d). The net current (Figure 3e) is the sum of the two opposite contributions. As the magnitude of the currents driven by the F-region wind dynamo is larger, the net downward current follows the signature of that current component.

4.2. Phase Delays of the Lunitidal Modulation

[23] In this subsection we calculate the lunitidal phases of the F-region vertical current density and various ionospheric quantities (EEJ, CTR, E_z/B_x, westward wind, and F-region vertical current). In the following discussion we assume that the 13-day oscillation originates from the semi-diurnal lunar tide [*Park et al.*, 2012] in order to discuss our results in relation with those of *Park et al.* [2012]. However, the generality of our main conclusion will not be affected by this assumption.

[24] We take a 40-day segment (∼13.26 × 3 days) of CHAMP observations around the SSW event; the EEJ, the F-region vertical current density, the westward neutral wind speed, the CTR of plasma density, and eastward plasma drift speed, respectively. The 'westward' wind and 'eastward' plasma drift directions were chosen because they both contribute to 'downward' currents in the equatorial F-region. Then a Discrete Fourier Transform (DFT) is applied to each data set after linear detrend. From the phase of the DFT we can calculate the delayed appearance of the tidal maximum at noon time with respect to the new/full moon epoch (hereafter, 'phase delay'); details of the calculation method are given in *Park et al.* [2012]. Let us take the EEJ as an example for modulation by the semi-diurnal lunar tide. During one semi-monthly period (=29.53/2 [days]) the noontime EEJ intensity peaks D days after the new/full moon epoch. In that case we say, "the phase delay of the lunitidal EEJ oscillation is D days."

[25] Phase delays of various ionospheric quantities (EEJ, CTR, E_z/B_x, westward wind, and F-region vertical current), which are obtained by applying the DFT to the ionospheric parameters, are listed in Table 1. Note that the EEJ, CTR, westward wind, and F-region vertical current are all observed by CHAMP while E_z/B_x is derived by inserting CHAMP observations into equation (3). Figure 4 shows schematically the wavefront propagation of lunitidal signatures for the ionospheric quantities. The phase delay for the EEJ is 4.7 days (or 3.8 lunar hours) from the new/full moon, which is compatible with the average value of 4.4 days in *Park et al.* [2012]. The phase delay for the CTR of the ionospheric density is 3.4 days (or 2.7 lunar hours). The relative delay between the EEJ and CTR is in qualitative agreement with the delayed response of the ionospheric plasma density to the vertical plasma drift (or equivalently to the EEJ) [e.g., *Stolle et al.*, 2008]; when comparing the curves in Figure 4 at a fixed moon phase. For the F-region vertical current we obtain a phase delay of about 0.6 days (or 0.5 lunar hours), which is neither in-phase nor anti-phase with that of the CTR.

[26] We find a weak but non-negligible variation of the F-region zonal wind at 400 km altitude with a period of ∼13 days (Figure 2b). The lunitidal phase delay of the westward thermospheric wind is about 2.7 days (or 2.2 lunar hours). The phase delay of the eastward plasma drift at the equator (E_z/B_x), which is estimated from equation (3), is about 11.6 days (or 9.4 lunar hours). The value is quite different from that of the F-region vertical current density, reflecting the nearly opposite phases of E_z/B_x and j_{down} in Figures 3c and 3e. In total, the lunitidal phase delay of the F-region vertical current (∼0.6 days) is different from all the other phase delays mentioned above. Hence, the conspicuous lunitidal modulation of the F-region vertical current during the SSW event in December 2001 results from a complex interaction between the F-region plasma density, electric field (probably of E-region origin), and thermospheric wind, each of which is affected by the lunar semi-diurnal tide with a different phase delay. This conclusion is in line with the one *Park et al.* [2010] have drawn for the phase of the non-migrating solar tidal wave signatures in the F-region vertical currents.

5. Summary

[27] During the SSW event of December 2001 CHAMP observations of zonal neutral wind, neutral/plasma density,

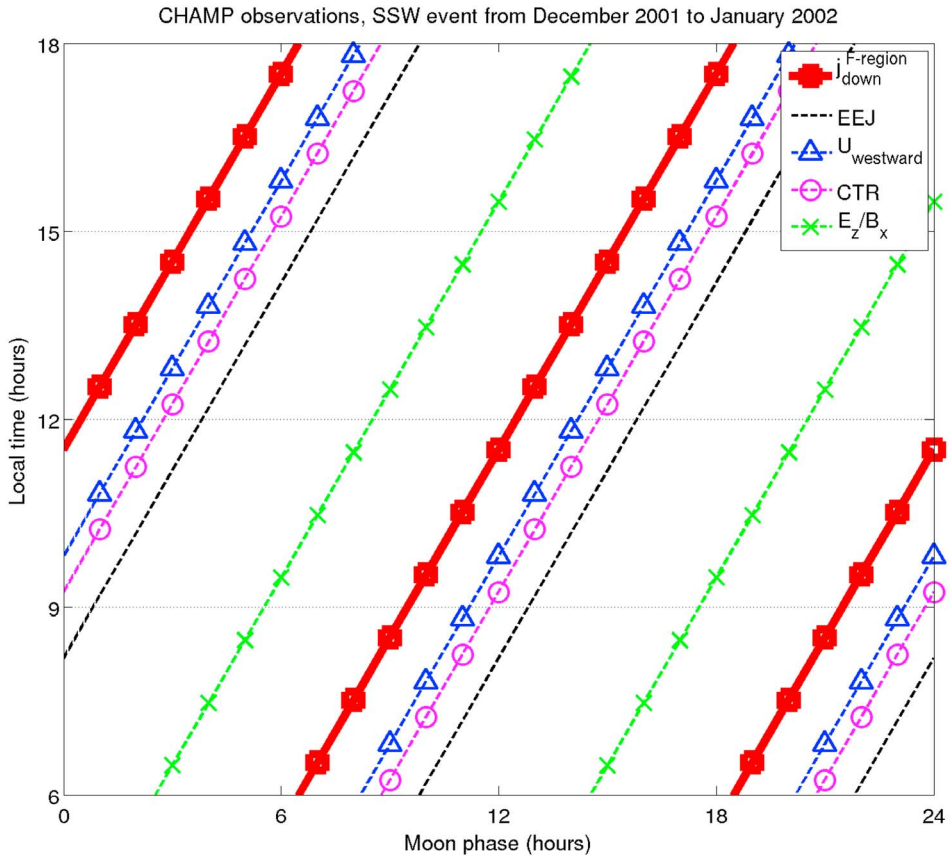

Figure 4. A schematic diagram showing the wavefront propagation of the semi-diurnal lunitidal signature of the EEJ, F-region vertical current density, westward wind speed, CTR of the F-region plasma density, and eastward plasma drift speed (E_z/B_x).

and geomagnetic field revealed the following features associated with the F-region vertical currents.

[28] 1. For the SSW onset of December 2001 we show that the vertical current density in the daytime equatorial F-region, as recorded by the CHAMP/FGM, is modulated at a 13-day period. The shape and period are consistent with the EEJ intensity modulation which has been attributed to the lunar semi-diurnal tide by *Park et al.* [2012].

[29] 2. Also the zonal neutral wind at CHAMP altitudes is modulated with an oscillation period comparable to that of the F-region vertical current. It implies that the upper thermospheric winds are significantly modulated by the lunar tide during an SSW event. The winds are expected to play the primary role in modulating the F-region vertical currents.

[30] 3. Zonal plasma drift in the equatorial F-region can be estimated from the magnetic and plasma/neutral observations of CHAMP. The obtained values are in qualitative agreement with the known climatology at Jicamarca [*Fejer et al.*, 2005], and also show quasi 13-day modulations. It implies that the zonal plasma drift in the equatorial F-region (probably caused by the wind dynamo in the E-region) is also modulated by the lunar tide during an SSW event.

[31] 4. From the observed phase delays of the lunitidal signatures we conclude that the modulation of the F-region vertical current is not only driven by the variation of the thermospheric wind, but also modulated by the E-region electric field and the F-region plasma density distribution (i.e., the modulated fountain effect and the resulting modulation of the F-region plasma density).

[32] **Acknowledgments.** The authors acknowledge valuable discussions with B. G. Fejer. The authors are grateful to S. Maus for providing the equatorial electrojet data, to C. Xiong for calculating the crest-to-trough ratio from the CHAMP/PLP data, and to M. Kunze for supplying the stratospheric temperature data. The OMNI data were obtained from the GSFC/SPDF OMNIWeb interface at http://omniweb.gsfc.nasa.gov. Wavelet software was provided by C. Torrence and G. Compo and is available at http://paos.colorado.edu/research/wavelets/. The CHAMP mission was sponsored by the Space Agency of the German Aerospace Center (DLR) through funds of the Federal Ministry of Economics and Technology, following a decision of the German Federal Parliament (grant code 50EE0944). The data retrieval and operation of the CHAMP satellite by the German Space Operations Center (GSOC) is acknowledged.

[33] Robert Lysak thanks the reviewers for their assistance in evaluating this paper.

References

Anderson, D., and E. A. Araujo-Pradere (2010), Sudden stratospheric warming event signatures in daytime E × B drift velocities in the Peruvian and Philippine longitude sectors for January 2003 and 2004, *J. Geophys. Res.*, *115*, A00G05, doi:10.1029/2010JA015337.

Brown, G. M. (1975), Sq variability and aeronomic structure, *J. Atmos. Terr. Phys.*, *37*, 107–117.

Brown, G. M., and D. C. Williams (1971), Pressure variations in the stratosphere and ionosphere, *J. Atmos. Terr. Phys.*, *33*, 1321–1328.

Chau, J. L., B. G. Fejer, and L. P. Goncharenko (2009), Quiet variability of equatorial E B drifts during a sudden stratospheric warming event, *Geophys. Res. Lett.*, *36*, L05101, doi:10.1029/2008GL036785.

Chau, J. L., L. P. Goncharenko, B. G. Fejer, and H.-L. Liu (2011), Equatorial and low latitude ionospheric effects during sudden stratospheric warming

events: Ionospheric effects during SSW periods, *Space Sci. Rev.*, *168*, 385–417, doi:10.1007/s11214-011-9797-5.

Dee, D. P., et al. (2011), The ERA-Interim reanalysis: configuration and performance of the data assimilation system, *Q. J. R. Meteorol. Soc.*, *137*, 553–597, doi:10.1002/qj.828.

Fang, T.-W., T. Fuller-Rowell, R. Akmaev, F. Wu, H. Wang, and D. Anderson (2012), Longitudinal variation of ionospheric vertical drifts during the 2009 sudden stratospheric warming, *J. Geophys. Res.*, *117*, A03324, doi:10.1029/2011JA017348.

Fejer, B. G., J. R. Souza, A. S. Santos, and A. E. Costa Pereira (2005), Climatology of F region zonal plasma drifts over Jicamarca, *J. Geophys. Res.*, *110*, A12310, doi:10.1029/2005JA011324.

Fejer, B. G., M. E. Olson, J. L. Chau, C. Stolle, H. Lühr, L. P. Goncharenko, K. Yumoto, and T. Nagatsuma (2010), Lunar-dependent equatorial ionospheric electrodynamic effects during sudden stratospheric warmings, *J. Geophys. Res.*, *115*, A00G03, doi:10.1029/2010JA015273.

Fejer, B. G., B. D. Tracy, M. E. Olson, and J. L. Chau (2011), Enhanced lunar semidiurnal equatorial vertical plasma drifts during sudden stratospheric warmings, *Geophys. Res. Lett.*, *38*, L21104, doi:10.1029/2011GL049788.

Fuller-Rowell, T., H. Wang, R. Akmaev, F. Wu, T.-W. Fang, M. Iredell, and A. Richmond (2011), Forecasting the dynamic and electrodynamic response to the January 2009 sudden stratospheric warming, *Geophys. Res. Lett.*, *38*, L13102, doi:10.1029/2011GL047732.

Goncharenko, L. P., J. L. Chau, H.-L. Liu, and A. J. Coster (2010a), Unexpected connections between the stratosphere and ionosphere, *Geophys. Res. Lett.*, *37*, L10101, doi:10.1029/2010GL043125.

Goncharenko, L. P., A. J. Coster, J. L. Chau, and C. E. Valladares (2010b), Impact of sudden stratospheric warmings on equatorial ionization anomaly, *J. Geophys. Res.*, *115*, A00G07, doi:10.1029/2010JA015400.

Häusler, K., H. Lühr, M. E. Hagan, A. Maute, and R. G. Roble (2010), Comparison of CHAMP and TIME-GCM nonmigrating tidal signals in the thermospheric zonal wind, *J. Geophys. Res.*, *115*, D00I08, doi:10.1029/2009JD012394.

Heelis, R. A., G. Crowley, F. Rodrigues, A. Reynolds, R. Wilder, I. Azeem, and A. Maute (2012), The role of zonal winds in the production of a prereversal enhancement in the vertical ion drift in the low latitude ionosphere, *J. Geophys. Res.*, *117*, A08308, doi:10.1029/2012JA017547.

Köhnlein, W. (1986), A model of the electron and ion temperatures in the ionosphere, *Planet. Space Sci.*, *34*, 609–630.

Lin, C. H., J. T. Lin, L. C. Chang, J. Y. Liu, C. H. Chen, W. H. Chen, H. H. Huang, and C. H. Liu (2012), Observations of global ionospheric responses to the 2009 stratospheric sudden warming event by FORMOSAT-3/COSMIC, *J. Geophys. Res.*, *117*, A06323, doi:10.1029/2011JA017230.

Liu, H., H. Lühr, S. Watanabe, W. Köhler, V. Henize, and P. Visser (2006), Zonal winds in the equatorial upper thermosphere: Decomposing the solar flux, geomagnetic activity, and seasonal dependencies, *J. Geophys. Res.*, *111*, A07307, doi:10.1029/2005JA011415.

Liu, H.-L., W. Wang, A. D. Richmond, and R. G. Roble (2010), Ionospheric variability due to planetary waves and tides for solar minimum conditions, *J. Geophys. Res.*, *115*, A00G01, doi:10.1029/2009JA015188.

Liu, H., M. Yamamoto, S. Tulasi Ram, T. Tsugawa, Y. Otsuka, C. Stolle, E. Doornbos, K. Yumoto, and T. Nagatsuma (2011), Equatorial electrodynamics and neutral background in the Asian sector during the 2009 stratospheric sudden warming, *J. Geophys. Res.*, *116*, A08308, doi:10.1029/2011JA016607.

Lühr, H., S. Maus, and M. Rother (2004), Noon-time equatorial electrojet: Its spatial features as determined by the CHAMP satellite, *J. Geophys. Res.*, *109*, A01306, doi:10.1029/2002JA009656.

Lühr, H. and S. Maus (2006), Direct observation of the F region dynamo currents and the spatial structure of the EEJ by CHAMP, *Geophys. Res. Lett.*, *33*, L24102, doi:10.1029/2006GL028374.

Pancheva, D., and P. Mukhtarov (2011), Global response of the ionosphere to atmospheric tides forced from below: Recent progress based on satellite measurements, *Space Sci. Rev.*, *168*, 175–209, doi:10.1007/s11214-011-9837-1.

Park, J., H. Lühr, and K. W. Min (2010), Characteristics of F-region dynamo currents deduced from CHAMP magnetic field measurements, *J. Geophys. Res.*, *115*, A10302, doi:10.1029/2010JA015604.

Park, J., H. Lühr, and K. W. Min (2011), Inter-hemispheric field-aligned currents in the ionosphere, *Ann. Geophys.*, *29*, 573–582, doi:10.5194/angeo-29-573-2011.

Park, J., H. Lühr, M. Kunze, B. G. Fejer, and K. W. Min (2012), Effect of sudden stratospheric warming on lunar tidal modulation of the equatorial electrojet, *J. Geophys. Res.*, *117*, A03306, doi:10.1029/2011JA017351.

Pedatella, N. M., and J. M. Forbes (2010), Evidence for stratosphere sudden warming-ionosphere coupling due to vertically propagating tides, *Geophys. Res. Lett.*, *37*, L11104, doi:10.1029/2010GL043560.

Ritter, P., H. Lühr, J. Park, C. Stolle, and C. Xiong (2012), Lunar signals in the variations of the daytime equatorial ionisation anomaly from CHAMP, paper presented at 13th International Symposium on Equatorial Aeronomy, Int. Symp. on Equat. Aeron., Paracas, Peru.

Rodrigues, F. S., G. Crowley, S. M. I. Azeem, and R. A. Heelis (2011), C/NOFS observations of the equatorial ionospheric electric field response to the 2009 major sudden stratospheric warming event, *J. Geophys. Res.*, *116*, A09316, doi:10.1029/2011JA016660.

Schunk, R. W., and A. F. Nagy (2009), *Ionospheres: Physics, Plasma Physics, and Chemistry*, 2nd ed., Cambridge Univ. Press, Cambridge, U. K.

Sridharan, S., S. Sathishkumar, S. Gurubaran (2009), Variabilities of mesospheric tides and equatorial electrojet strength during major stratospheric warming events, *Ann. Geophys.*, *27*, 4125–4130.

Stening, R. J. (1992), The enigma of the counter equatorial electrojet and lunar tidal influences in the equatorial region, *Adv. Space Res.*, *12*(6), 23–32.

Stening, R. J. (2011), The lunar tide in the equatorial electrojet in relation to stratospheric warmings, *J. Geophys. Res.*, *116*, A12315, doi:10.1029/2011JA017047.

Stolle, C., C. Manoj, H. Lühr, S. Maus, and P. Alken (2008), Estimating the daytime Equatorial Ionization Anomaly strength from electric field proxies, *J. Geophys. Res.*, *113*, A09310, doi:10.1029/2007JA012781.

Yamazaki, Y., A. D. Richmond, and K. Yumoto (2012a), Stratospheric warmings and the geomagnetic lunar tide: 1958–2007, *J. Geophys. Res.*, *117*, A04301, doi:10.1029/2012JA017514.

Yamazaki, Y., K. Yumoto, D. McNamara, T. Hirooka, T. Uozumi, K. Kitamura, S. Abe, and A. Ikeda (2012b), Ionospheric current system during sudden stratospheric warming events, *J. Geophys. Res.*, *117*, A03334, doi:10.1029/2011JA017453.

Yue, X., W. S. Schreiner, J. Lei, C. Rocken, D. C. Hunt, Y.-H. Kuo, and W. Wan (2010), Global ionospheric response observed by COSMIC satellites during the January 2009 stratospheric sudden warming event, *J. Geophys. Res.*, *115*, A00G09, doi:10.1029/2010JA015466.